Magnetocaloric properties and unconventional critical behavior in $(Gd,Tb)_6(Fe,Mn)Bi_2$ intermetallics

A. Oleaga [a, *], A. Herrero [a], A Salazar [a], A.V. Garshev [b], V. O. Yapaskurt [c], A.V. Morozkin [b]

[a] Departamento de Física Aplicada I, Escuela de Ingeniería de Bilbao, Universidad del País Vasco UPV/EHU, Plaza Torres Quevedo 1, 48013 Bilbao, Spain
[b] Department of Chemistry, Moscow State University, Lenisnkie Gory, House 1, Building 3, Moscow, GSP-2, 119991, Russia
[c] Department of Petrology, Geological Faculty, Moscow State University, Leninskie Gory, Moscow, 119991, Russia

ABSTRACT

The magnetic and magnetocaloric properties of the intermetallic family $(Gd,Tb)_6(Fe,Mn)Bi_2$ have been studied from 2 K to temperatures above the respective Curie temperatures T_C. The substitution of Gd by Tb (Gd_6FeBi_2, $Gd_3Tb_3FeBi_2$, Tb_6FeBi_2) tunes T_C in the range 350-250 K and favors the apparition of a metamagnetic transition at very low temperature (below 10 K) from a complex magnetic state to a ferromagnetic one, as well as a spin reorientation transition below T_m = 72 K. As a consequence, an important inverse magnetocaloric effect (IMCE) appears below 20 K and an interesting direct magnetocaloric effect (DMCE) appears over a wide temperature span between T_C and T_m with maxima at those temperatures. The partial substitution of Fe by Mn in $Tb_6Fe_{0.5}Mn_{0.5}Bi_2$ shifts these effects upwards in temperature while expanding the region of the direct magnetocaloric effect between 70 and 400 K. The combination of adjoint IMCE and DMCE as well as the wide span of the latter shows that tuning this family allows to locate the magnetocaloric effect in different regions of interest. The critical behavior of the PM-FM transitions has been studied obtaining the critical exponents α, β, γ, δ and checking that the respective magnetocaloric effects also scale with the critical parameters n and δ. The transition in Gd_6FeBi_2 belongs to the Heisenberg universality class with deviations due to magnetocrystalline anisotropies; the critical exponents for $Gd_3Tb_3FeBi_2$ (in agreement with the Mean Field model) suggest the presence of long range order magnetic interactions, while Tb_6FeBi_2 and $Tb_6Fe_{0.5}Mn_{0.5}Bi_2$ present an unconventional critical behavior aligned with long range order interactions.

Keywords: Magnetocaloric effect; Rare earth compound; Magnetic properties; Spin-ordering; Critical behavior

*Corresponding author; E-mail: alberto.oleaga@ehu.es

1. Introduction

The study of intermetallic materials has boosted in the last decade since more and more different compositions are grown and found to show interesting and complex magnetic properties, some of which can be used for practical applications. One of the most promising fields is related to the development of new materials for energy applications and, in particular, with a relevant magnetocaloric effect. Magnetocaloric materials are the core of the new refrigeration technology which intends to compete with and eventually substitute the current gas compressor-expansion technology [1-3]. Therefore, intensive research is carried out searching for suitable magnetocaloric materials in several temperature regions, from the different gas liquefaction regions to room temperature [4-8]. For practical applications, a "suitable" magnetocaloric material needs to present a magnetic transition with no hysteresis (neither thermal nor magnetic), a high magnetic entropy change (spanning over a wide as possible temperature change) and a high value of the refrigerant capacity. Obviously, there is a huge effort focused on room temperature, where several materials have already been found to be likely candidates, such as pure Gd and Ge-containing compounds, manganites, Heusler alloys, etc. [9-17]. Another focus is to tune the magnetocaloric properties of certain compounds playing with their chemical composition in order to build up multi-component compounds, as it has been shown to be the case for $(Tb_{1-x}Dy_x)FeSi$ (x from 0 to 1) [18] or R_2T_2X (R = Gd-Tm; T = Cu, Ni, Co; X = Cd, In, Ga, Sn, Al) [4]. In particular, we showed in a previous paper that changing the percentage of Fe and Mn in the intermetallics $Ho_6(Mn,Fe)Bi_2$ allows to extend the width of the operating temperature range with a nearly constant value of the magnetic entropy change, due to the presence of two magnetic transitions, as well as tuning the temperature at which the magnetic entropy change is maximum [19]. The purpose of this paper is to look for another branch of this family of R_6TBi_2 compounds (R=rare earth, T=transition metal) whose tuning can make them operative in the room temperature range as well as at low temperature, presenting a wide temperature span due to the possible presence of several magnetic

transitions. To this end, we have focused our attention on Gd_6FeBi_2, $Gd_3Tb_3FeBi_2$, Tb_6FeBi_2 and $Tb_6(Fe_{0.5}Mn_{0.5})Bi_2$. The crystal structure and some magnetic properties have already been studied for both Gd_6FeBi_2 and Tb_6FeBi_2 [20-26] while a comprehensive study on the magnetic and magnetocaloric properties of the four aforementioned compositions will give a broader view of the general properties of the family and the role of the different ions, leading the path to appreciate their feasibility for practical applications.

As a knowledge in depth of the magnetic properties is fundamental prior to any possible practical application, the purpose of this paper is to obtain it by means of the study of the critical behavior of the second-order paramagnetic-ferromagnetic transition that these compounds are known to present at a relatively high temperature, obtaining a whole set of critical parameters ($\alpha, \beta, \gamma, \delta, n$) related to the scaling of the following physical measurables:

$$c_p(T) \sim A^{\pm}|t|^{-\alpha} \qquad (A^- \text{for } T < T_C,\ A^+ \text{for } T > T_C), \tag{1}$$

$$M_S(T) \sim |t|^{\beta} \qquad (T < T_C), \tag{2}$$

$$\chi_0^{-1}(T) \sim |t|^{\gamma} \qquad (T > T_C), \tag{3}$$

$$M(H) \sim H^{1/\delta} \qquad (T = T_C), \tag{4}$$

$$\Delta S_M^{pk} \sim H^{1+(1/\delta)(1-1/\beta)} = H^n \tag{5}$$

where T_C is the Curie temperature, $c_p(T)$ the specific heat, $M_S(T)$ the spontaneous magnetization, $\chi_0(T)$ the initial susceptibility, $M(H)$ $(T=T_c)$ the critical isotherm, ΔS_M^{pk} the maximum of the magnetic entropy change and $t = (T-T_C)/T$ the reduced temperature; besides, the magnetic equation of state

$$M(H, t) = |t|^{\beta} f_{\pm}(H/|t|^{\beta+\gamma}) \tag{6}$$

must be fulfilled in the critical region [27-30].

The expectation is that the obtained values of the critical parameters will allow us to assign an already theorized universality class to the magnetic transition (or a nearness to one of them), so that a deeper insight in the physics of the magnetic properties will be revealed. Moreover, the complete study of the magnetocaloric properties of the four compounds presented in this study, including the refrigerant capacity, as well as the possibility to obtain universal curves from the magnetic entropy change, will fully characterize their ability to be used as magnetocaloric materials.

2. Samples and experimental techniques

Alloys with a total mass of 2 g were prepared by arc-melting in an electric arc furnace (90 V, 150 A) under argon (99.992 vol. %) using a non-consumable tungsten electrode and on a water-cooled copper hearth. Pieces of gadolinium, terbium (99.9 wt. %), iron, manganese (99.95 wt. %) and bismuth (purity 99.99 wt.%) were used as starting components. A titanium button was used as a getter during arc-melting and the alloys were remelted three times. The arc-melted samples were wrapped into nickel foil and sealed in silica ampoules, evacuated and back filled with argon to 0.3 atm at room temperature. The samples were annealed at 1070 K (± 2 K) for 300 hours to synthesize Fe_2P-type polycrystals via solid state reaction by a diffusion process from an initial mixture of rare earth, $R\{Fe, Mn\}_2$ and R_5Bi_3 compounds, then quenched in ice-water bath.

Phase analysis of the alloys was carried out using X-ray diffraction and energy dispersive X-ray spectroscopy microprobe elemental analysis (EDS). The X-ray powder data (XRD) were obtained by using a diffractometer Rigaku D/MAX-2500 (CuKα, 2θ of 10-80º, 0.02º step, $I_{max}/I_{bgr} \sim 50$). An INCA-Energy-350 X-ray EDS spectrometer (Oxford Instruments) on a Jeol JSM-6480LV scanning electron microscope (SEM) (20 kV accelerating voltage, 0.7 nA beam current and 50 μm beam diameter, microprobe size ~ 10 nm) was employed to perform quantitative elemental analysis. Signals averaged over three points per phase gave estimated standard deviations of 0.5 at.% for gadolinium and terbium (measured by L-series lines), 1 at.% for Mn, Fe and Bi (measured by K-series lines).

The unit cell data were derived from powder X-ray data using the Rietan-program [31] in the isotropic approximation at room temperature.

Magnetic measurements have been performed using a VSM (Vibrating Sample Magnetometer) by Cryogenic Limited, obtaining the magnetization (M) of the samples under external applied magnetic fields H_a in the range of 0 to 7 T. Isotherms have been collected from very low temperatures to temperatures well above the corresponding Curie temperature (T_C) for all samples, using different steps, depending on the temperature range. In order to study the critical behaviour of the paramagnetic to ferromagnetic transition in detail, a step of $\Delta T = 1$ K has been taken between consecutive isotherms around T_C. Demagnetization effects have been taken into account in order to perform a correct evaluation of the scaling analysis and the magnetocaloric effect [32, 33], thus obtaining the internal magnetic field $H_i = H_a - NM$, where N is the demagnetization

factor, which has been obtained from zero-field *ac* susceptibility measurements following the method described in [34, 35], extracting the maximum value of this magnitude (often referred as the Hopkinson/principal maximum) and using the relation $N=1/\chi_{max}$.

The magnetic susceptibility was measured with AC Measurement System Option in PPMS (Physical Properties Measurement System) by Quantum Design.

The specific heat has been retrieved using a high resolution *ac* photopyroelectric calorimeter in the back detection configuration, which allows to perform extremely slow temperature ramps in order to extract the shape of c_p with great accuracy, to be used to study the critical behaviour of the paramagnetic to ferromagnetic transitions for all samples [36-38].

3. Experimental results and discussion

The X-ray powder analysis showed that Gd_6FeBi_2, $Gd_3Tb_3FeBi_2$, Tb_6FeBi_2 and $Tb_6Mn_{0.5}Fe_{0.5}Bi_2$ (‘$Gd_{67.1(8)}Fe_{10.6(8)}Bi_{22.1(7)}$', '$Gd_{34.7(8)}Tb_{32.6(7)}Fe_{10.1(8)}Bi_{22.6(6)}$', '$Tb_{66.9(8)}Fe_{10.5(8)}Bi_{22.6(6)}$' and '$Tb_{67.1(9)}Mn_{5.7(6)}Fe_{4.7(6)}Bi_{22.5(6)}$' compositions from microprobe analysis, respectively) crystallize in the Fe_2P-type structure (space group $P\bar{6}2m$, No. 189, *hP*9). The refined unit cell data and atomic positions are given in Table 1. The substitution of Fe for Mn is followed via increasing of unit cell volume and anisotropic distortion of unit cell (increasing of *c*/*a* ratio) from Tb_6FeBi_2 to $Tb_6Mn_{0.5}Fe_{0.5}Bi_2$. Meanwhile, the substitution of Tb for Gd leads to almost isotropic expansion of unit cell from Tb_6FeBi_2 to $Gd_3Tb_3FeBi_2$ and Gd_6FeBi_2 (increasing of unit cell volume, while *c*/*a* ratio is close to constant).

Fig.1 shows the Rietveld refinement and SEM photograph of $Tb_6Mn_{0.5}Fe_{0.5}Bi_2$, as an example. Since these compounds are synthesized through a diffusion process, as explained in detail in [39], the alloys contain an admixture of Yb_5Sb_3-type $(Gd,Tb)_5(Fe,Mn)_{\sim 0.5}Bi_{\sim 2.5}$ phases (8-10 wt %) (see Table 1s in Supplementary material for details). The admixture of Yb_5Sb_3-type Gd_5Bi_3 exhibits ferromagnetic ordering around 110 K [40] and admixture of Yb_5Sb_3-type Tb_5Bi_3 may show ferromagnetic ordering around 70 K in accordance with de Gennes rule [41]. Meanwhile these admixtures show a small influence for the resulting magnetic properties, as will be discussed later.

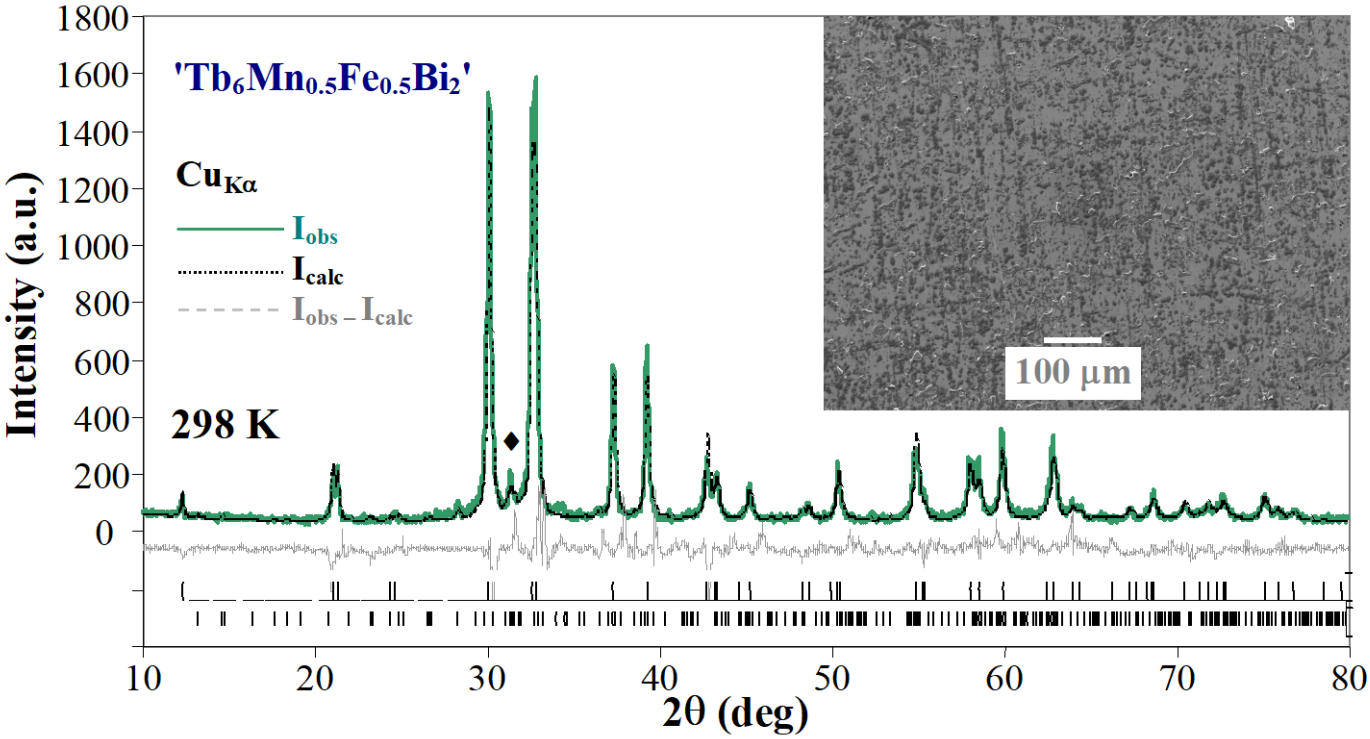

Fig. 1. Rietveld refinement of the X-ray powder pattern and SEM photo of the '$Tb_6Mn_{0.5}Fe_{0.5}Bi_2$': alloy contains ~91 wt.% of Fe_2P-type $Tb_6Mn_{0.5}Fe_{0.5}Bi_2$ (R_F = 5.6 %) ($Tb_{67.1(9)}Mn_{5.7(6)}Fe_{4.7(6)}Bi_{22.5(6)}$ from X-ray spectral analysis: white-grey phase) and ~9 wt. % of Yb_5Sb_3-type $Tb_5Fe_{0.22}Mn_{0.08}Bi_{2.7}$ (R_F = 6.2 %) ($Tb_{63.9(9)}Mn_{1.0(4)}Fe_{2.1(9)}Bi_{33.0(9)}$ from X-ray spectral analysis: dark-grey phase). The first and second rows of ticks refer to the diffraction peaks of $Tb_6Mn_{0.5}Fe_{0.5}Bi_2$ and $Tb_5Fe_{0.22}Mn_{0.08}Bi_{2.7}$, respectively. The strongest peak of admixture Yb_5Sb_3-type $Tb_5Fe_{0.22}Mn_{0.08}Bi_{2.7}$ is marked in Figure (♦).

Fig. 2 shows the magnetization as a function of temperature, both in Zero-Field Cooled (ZFC) and Field-Cooled (FC) mode for the four samples, with an applied field of 100 Oe. In all samples with Tb, there is a clear divergence between the ZFC and FC curves, showing thermomagnetic irreversibility, typical of many ferromagnetic (or ferrimagnetic) transitions. While Gd_6FeBi_2 has only a paramagnetic to ferromagnetic (PM-FM) transition at T_C = 346K, there are clearly two main transitions in the other compounds, with some intermediate minor transitions due to other residual phases (see, for instance, the transition at 144 K for $Tb_5Fe_{0.4}Bi_{2.6}$, present in the nominal compound Tb_6FeBi_2).

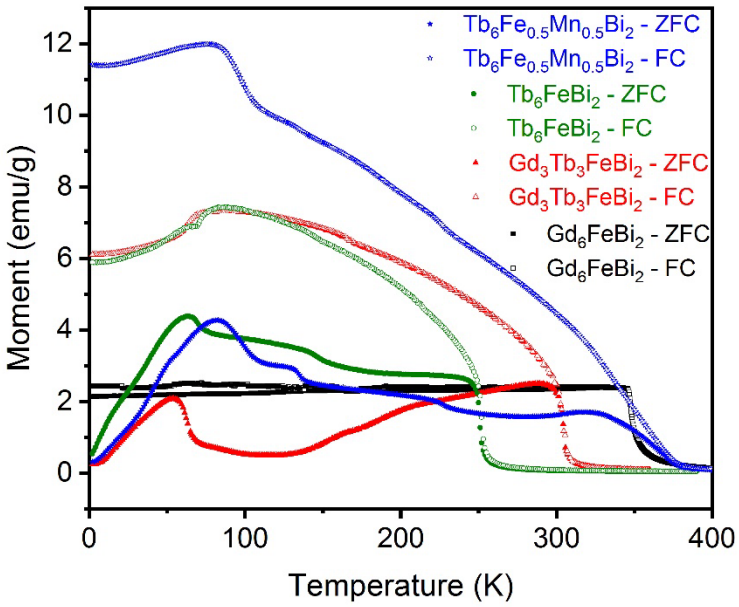

Fig 2. Magnetic moment as a function of temperature in zero-field cooled (ZFC) and field-cooled (FC) mode with applied field H = 100 Oe.

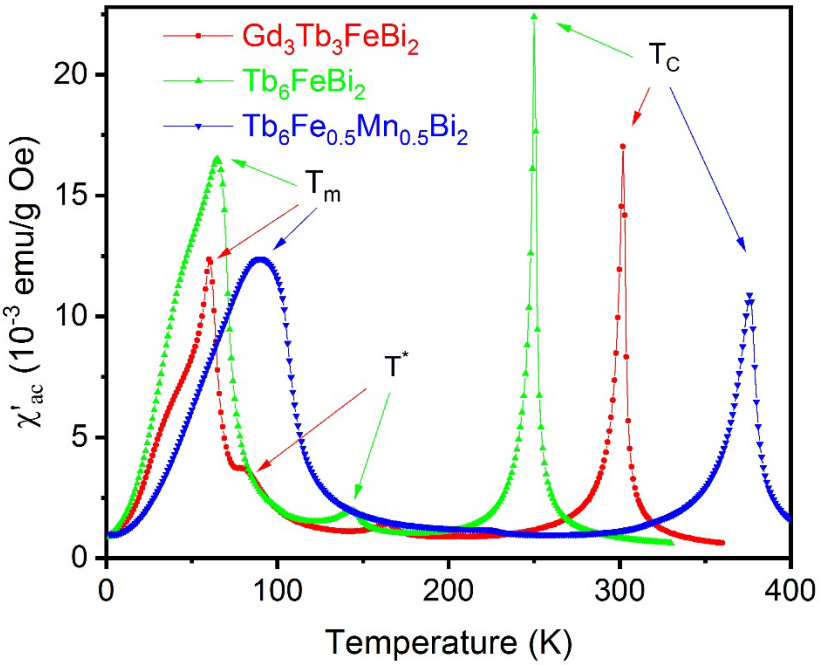

Fig 3. Real part of the *ac* susceptibility at f = 100Hz. T_C corresponds to the paramagnetic to ferromagnetic transitions, T_m to the spin reorientation ones, T^* to ferromagnetic transitions of the secondary phases.

The position of the transitions is clearly revealed in the *ac* susceptibility measurements, whose real part is represented in Fig. 3 (T^* corresponds to transitions for

the secondary phases). The substitution of Gd by Tb and Fe by Mn allows to tune the Curie temperature, which is placed at 302 K for $Gd_3Tb_3FeBi_2$, 250 K for Tb_6FeBi_2, and 376 K for $Tb_6Fe_{0.5}Mn_{0.5}Bi_2$, while there are spin-reorientation transitions placed at T_m = 60 K, 65 K and 90 K (for $Gd_3Tb_3FeBi_2$, Tb_6FeBi_2, and $Tb_6Fe_{0.5}Mn_{0.5}Bi_2$, respectively), which, as will be shown later, play a major role in the magnetocaloric properties of these compounds. The positions of T_C and T_m agree quite well with previous measurements in Gd_6FeBi_2 and Tb_6FeBi_2 [21, 22, 24]. The high-temperature ferromagnetic ordering corresponds to the *c*-axis collinear ferromagnetic ordering of rare earth sublattice, while low-temperature transition of Tb_6FeBi_2, $Gd_3Tb_3FeBi_2$ and $Tb_6Mn_{0.5}Fe_{0.5}Bi_2$ is attributed to an additional *ab*-plane ferro-antiferromagnetic component of the rare earth sublattice [39]. The presence of low temperature phases with complex spin arrangements which include canted ferromagnets, conical or spiral or simply antiferromagnetic is quite common in R_6TX_2 family, where no magnetic moment has been found for the transition metal [39, 42, 43]. Concerning the evolution of the magnetic properties, starting from Gd_6FeBi_2, the introduction of Tb to reach $Gd_3Tb_3FeBi_2$ and then Tb_6FeBi_2 provokes a monotonous evolution in the reduction of T_C, as well as in the general shape of the ZFC-FC curves, and it will be seen later that the magnetocaloric properties have a similar behavior. Adding Mn changes this tendency, taking the magnetic transitions to a higher temperature and separating more T_C from T_m, what it has already been observed in other compounds of the family when substituting Fe by Mn, as in Ho_6FeBi_2 and Dy_6FeBi_2 [19, 39].

The isothermal magnetizations at 2 K, shown in Fig 4, explain the origin of the differences between ZFC and FC curves for the samples containing Tb. In the case of Gd_6FeBi_2 there is a negligible coercive field H_C, while it is in the range 1-2 kOe for the other ones. Moreover, there is a step-like behavior in the latter, typical of metamagnetic transitions, which points to the presence of antiferromagnetic interactions responsible for a non-collinear magnetic structure at very low temperature. The fact there are several steps in two cases indicates the existence of intermediate magnetic arrangements till the final ferromagnetic state is reached. The low temperature magnetic state quickly turns into a ferromagnetic state as the temperature is raised, as it is seen in the evolution of the magnetization isotherms as a function of the applied field, where in a small temperature range (approximately 2-14K for $Gd_3Tb_3FeBi_2$, 2-20K for Tb_6FeBi_2, and 2-14K for $Tb_6Fe_{0.5}Mn_{0.5}Bi_2$) the magnetization has the general behavior of increasing from one isotherm to the next, higher one, for the same value of the magnetic field, confirming the

presence of antiferromagnetic interactions (see Fig. 5, where details are shown for the case of Tb_6FeBi_2 and $Tb_6Fe_{0.5}Mn_{0.5}Bi_2$); from then on, with increasing values of temperature, the behaviour of the isotherms is the common one for a ferromagnetic state, i.e., for a given applied field, the magnetization decreases as temperature is increased (see Fig. 5 for $Gd_3Tb_3FeBi_2$). In fact, one of them, $Tb_6Fe_{0.5}Mn_{0.5}Bi_2$ has even a more complicated behavior, as at very low temperature (< 3.5 K) the metamagnetic transition changes the ground state to a ferromagnetic one from an intermediate field, as it is also shown in Fig. 5.

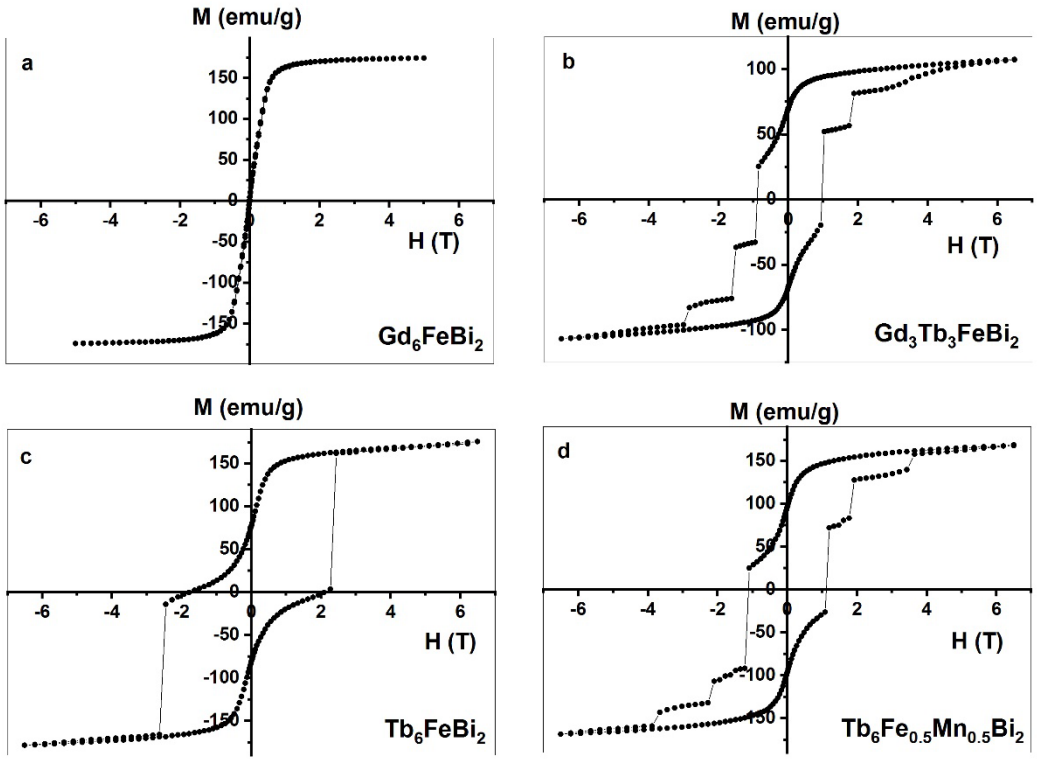

Fig. 4. Hysteresis loops at 2K: a) Gd_6FeBi_2 ; b) $Gd_3Tb_3FeBi_2$; c) Tb_6FeBi_2; d) $Tb_6Fe_{0.5}Mn_{0.5}Bi_2$.

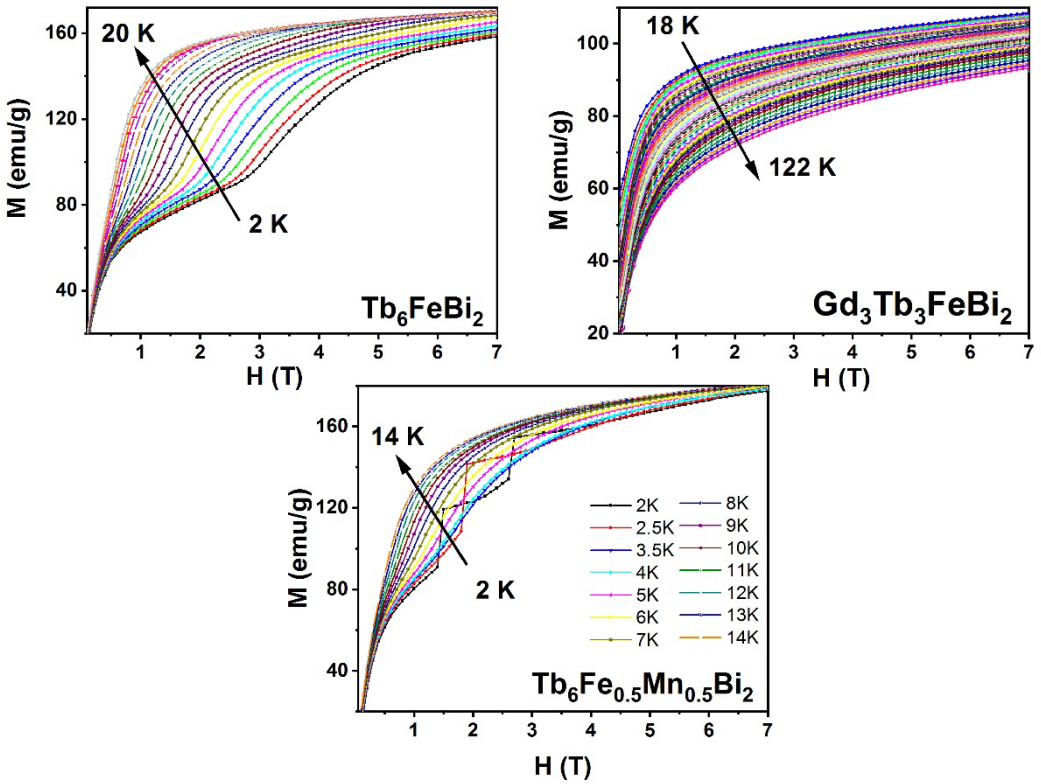

Fig. 5. Magnetization isotherms at low temperature for Tb_6FeBi_2 and $Tb_6Fe_{0.5}Mn_{0.5}Bi_2$; and at medium temperature for $Gd_3Tb_3FeBi_2$.

3.1. Critical behavior.

In order to extract the critical exponents β, γ, δ for the PM-FM transitions, detailed magnetization isotherms have been measured in the vicinity of the respective Curie temperatures. In the first place, an Arrot Plot (M^2 versus H/M) is plotted where, in order to maintain a simple notation, H is used instead of H_i to represent the internal field; this notation will be maintained all through the paper. If a perfect Mean Field model is of application, the curves, at high field, will be straight lines, parallel to each other. It is well known that many magnetic transitions belong to other universality class so that the curves would show these features on a Modified Arrott Plot, where $M^{1/\beta}$ is represented versus $(H/M)^{1/\gamma}$ with the appropriate values of the critical exponents. Table 2 shows their values for the most common universality classes and Fig. 6 shows the graphs for Mean Field (Fig. 6a), and Heisenberg (Fig. 6b) models for Gd_6FeBi_2. The one with best straight and parallel lines is the Heisenberg one, so this has been taken as a starting point to find the best values for β and γ (the Ising model has also been tested but the result is worse than for the Heisenberg case). A common iterative procedure has then been followed [44, 45]. A linear extrapolation from high field data on the MAP has been used to extract the $(M_S)^{1/\beta}$ and $(\chi_0^{-1})^{1/\gamma}$ values as the interception with Y and X axes, respectively. Once $M_S(T)$ and

$\chi_0^{-1}(T)$ have been obtained they are fitted to Eqs. (2) and (3) to obtain new values of β and γ, which are then used for another iteration until the values converge and good parallel, straight lines, are obtained in the MAP. The final result is shown in Fig. 6c and Table 3 contains the exponents with their errors. Fig. 6d shows the spontaneous magnetization and the inverse of the initial susceptibility vs. temperature as obtained from the optimized Modified Arrot Plot. The obtained β value is nearly the one for the Heisenberg model ($\beta_{exp} = 0.369$, $\beta_{Heis} = 0.365$) though γ is smaller ($\gamma_{exp} = 1.188$, $\gamma_{Heis} = 1.386$).

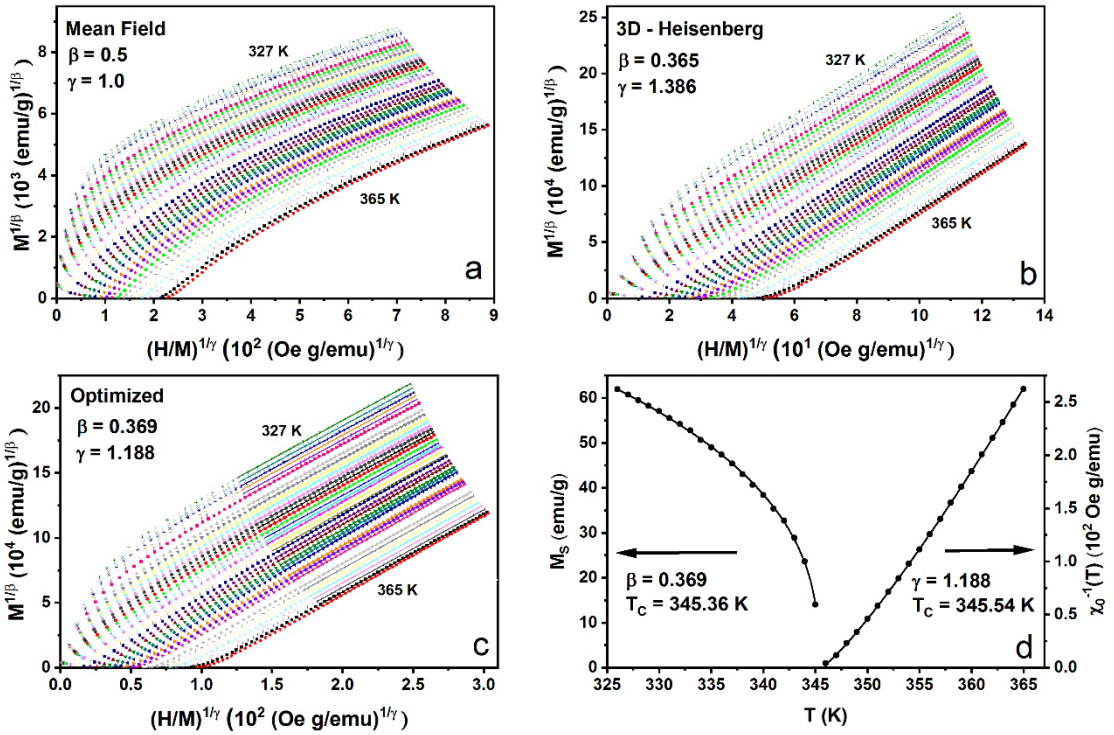

Fig 6. Gd_6FeBi_2: a) Arrot plot, corresponding to the Mean Field universality class parameters; b) Modified Arrot Plot for the 3D-Heisenberg class; c) Optimized Modified Arrot Plot; d) Spontaneous magnetization (left) and inverse of initial susceptibility (right) vs. temperature as obtained from the optimized Modified Arrot Plot.

In the case of the other three samples, which contain Tb, the situation is very different, while they share some common features. Fig 7a presents the Arrott Plot for $Tb_6Fe_{0.5}Mn_{0.5}Bi_2$ using the Mean Field model, which happens to be much better as a starting point than the Heisenberg or Ising models, but its critical exponents are not really the good ones. We have tested different sets of parameters close to the Mean Field model as starting points before proceeding with the iteration procedure and the final result is

shown in Fig 7b, where γ is indeed very close to the Mean Field value (γ_{exp} = 0.95, γ_{MF} = 1.0) while β takes the value of 0.72, higher than any proposed universality class. There is an intermediate situation for $Gd_3Tb_3FeBi_2$ and Tb_6FeBi_2 but in both cases the Mean Field model was a better choice as a starting trial than the Heisenberg or Ising ones. Substituting half of the Gd with Tb takes the critical exponents quite close to the Mean Field model (β_{exp} = 0.58, γ_{exp} = 1.01) (Fig. 7c) while completely substituting it moves them to farther values (β_{exp} = 0.73, γ_{exp} = 0.80, Fig. 7d).

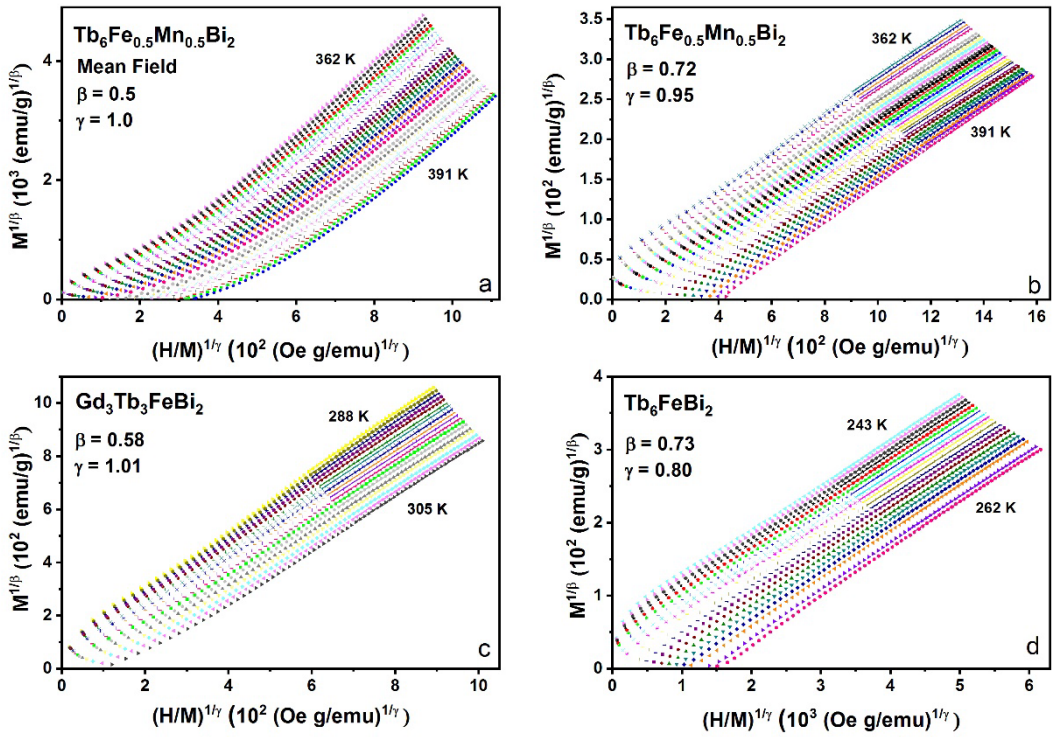

Fig 7. a) Arrot plot, corresponding to the Mean Field universality class parameters for $Tb_6Fe_{0.5}Mn_{0.5}Bi_2$; b) Optimized Modified Arrot Plot for $Tb_6Fe_{0.5}Mn_{0.5}Bi_2$; c) Optimized Modified Arrot Plot for $Gd_3Tb_3FeBi_2$; d) Optimized Modified Arrot Plot for Tb_6FeBi_2.

For the four compounds, the critical isotherms have been plotted to extract the critical exponent δ, after Eq. (4). Fig. 8 shows two of them in a log-log scale, where the points should be along a straight line, as it happens in all cases. From the slope, the value of δ is easily retrieved and can be compared with the one using the Widom scaling equation [30]:

$$\delta = 1 + \gamma/\beta \qquad (7)$$

We will call the result of this operation δ_{calc} while naming δ_{exp} the obtained ones from the graphs.

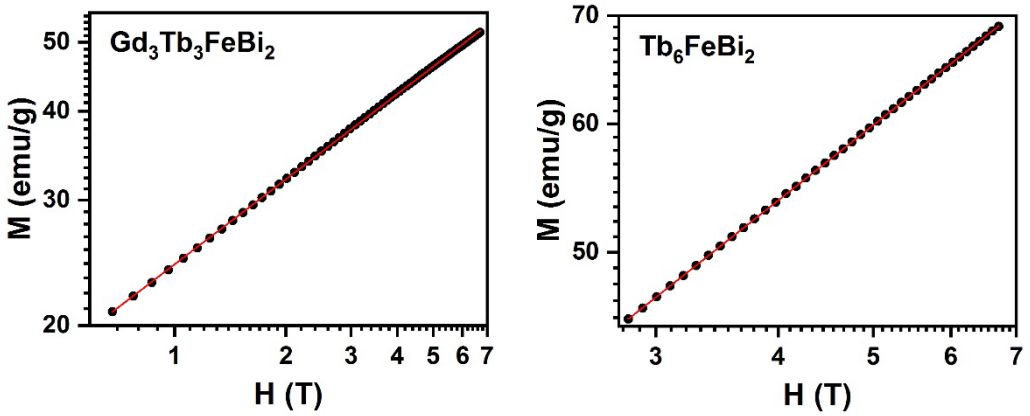

Fig. 8. *M* vs. *H* plot in a log-log scale collected at critical isotherms for $Gd_3Tb_3FeBi_2$ (left) and Tb_6FeBi_2 (right).The straight line, in each case, is the linear fit from which the exponent δ is obtained.

In all cases, the agreement is very good: δ_{exp} = 4.277 against δ_{calc} = 4.22 for Gd_6FeBi_2, δ_{exp} =2.618 vs δ_{calc} = 2.8 for $Gd_3Tb_3FeBi_2$, δ_{exp} = 2.087 vs δ_{calc} = 2.1 for Tb_6FeBi_2, and, finally, δ_{exp} = 2.251 vs δ_{calc} = 2.27 for $Tb_6Fe_{0.5}Mn_{0.5}Bi_2$. These results are also gathered in Table 3.

A confirmation of the validity of these critical exponents to describe the magnetic transition is the fulfilment of the magnetic equation of state Eq. (6). Fig. 9 has been built up with the critical exponents just obtained, for Gd_6FeBi_2 and $Tb_6Fe_{0.5}Mn_{0.5}Bi_2$, and it can be appreciated that all isotherms collapse onto two independent branches, one for those below T_C, a second one for those above it. This happens for the four compounds and is considered a strong confirmation of the validity of the critical exponents.

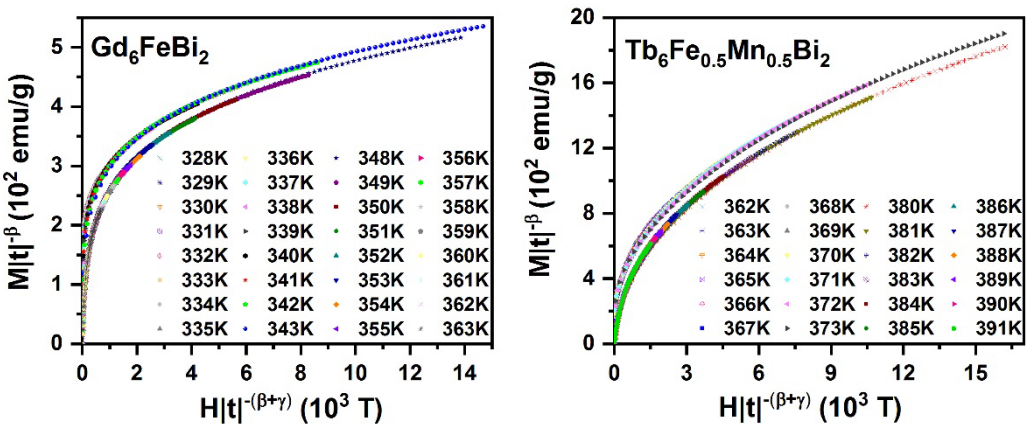

Fig. 9. The renormalized magnetization plotted as a function of the renormalized field following Eq. (6) for Gd_6FeBi_2 (left) and $Tb_6Fe_{0.5}Mn_{0.5}Bi_2$ (right). In each case, all data collapse in two separate branches, one above and one below the respective T_C.

Let's examine the obtained values of the critical exponents in some detail: We can see that, for the case of Gd_6FeBi_2, β agrees very well with the theoretical one for the Heisenberg case ($\beta_{exp} = 0.369$, $\beta_{Heis} = 0.365$) while γ and δ are smaller, though there is a good coherence among them, as they satisfy Eqs. (6) and (7). This implies that the magnetic interactions are short range though there is not a perfect isotropic distribution of the spins, which is the basis of this model. It is generally accepted that, in the general family R_6TBi_2, the T ions do not carry magnetic moments, as it has been proven by neutron diffraction in some of them [21, 24, 25, 42, 46] so the magnetism basically arises from the rare earth atoms by means of an indirect *4f-4f* interaction via the Ruderman-Kittel-Kasuya-Yosida (RKKY) interaction. The fact that the Curie temperatures are higher than what corresponds to the rare earth ion alone (for Gd $T_C = 292.77$ K [47] while for Gd_6FeBi_2 $T_C = 345.45$ K) is attributed to a hybridization phenomena between electronic orbitals of the rare earth and the other ions in the compound [1, 25, 48]. Gd and some Gd-based compounds present a PM-FM transition which is close to the 3D-Heisenberg universality class [49-51] though always with some deviations. The deviation that we have found can not have its origin in crystal field effects, as it happens with some other rare earths, because the orbital moment L is 0 for Gd, so it is surely due to some kind of magnetocrystalline anisotropy, such as a non-negligible spin-orbit coupling of the itinerant electrons, as it has been suggested for other Gd-based compounds [52-53].

The partial substitution of Gd by Tb and its complete substitution completely changes the scenario. $Gd_3Tb_3FeBi_2$ presents critical exponents very close to the Mean

Field model (β_{exp} = 0.58, γ_{exp} = 1.01), indicating that long range order interactions are now governing the transition; at the same time, the critical temperature is reduced around 50 K, while the complete substitution (Tb_6FeBi_2) reduces it another 40 K; in the latter, the critical exponents take values which do not comply with any universality class, with a growing β and a decreasing γ (β_{exp} = 0.73, γ_{exp} = 0.80). Besides (see Fig. 4), the introduction of Tb leads to the opening of the hysteresis loop, with a relevant coercive field, as well as to the appearance of metamagnetic transitions at low temperature, supporting the fact that the magnetism drastically changes with the presence of Tb. The reduction in T_C is due to the lower value of the total spin S for Tb compared to Gd, while the Tb non-zero orbital moment (L=3), as well as crystal field effects, introduce magnetocrystalline anisotropies [54]. The substitution of Fe by Mn in $Tb_6Fe_{0.5}Mn_{0.5}Bi_2$ only slightly modifies the values of the critical exponents (β_{exp} = 0.72, γ_{exp} = 0.95).

Since there is no universality class with β values bigger than 0.5 or γ smaller than 1.0, it is not evident to associate the values obtained here (0.72, 0.73 for β, 0.80, 0.95 for γ) to a particular distribution of spins or order of the interactions translated to a certain Hamiltonian, though the γ values suggest that it is a long-range interaction, as they are close to 1, and the values of β indicate a certain deviation from the Mean Field model, but it is difficult to understand the origin of this deviation. There are many other materials which have been also found to present an unconventional critical behaviour, with critical exponents around these values: $Sr_{1-x}A_xRuO_3$ [55, 56], $La_{0.5}Ca_{0.4}Ag_{0.1}MnO_3$ [57], $La_{0.4}Ca_{0.6}MnO_3$ [58], $BaIrO_3$ [59], κ-$(BEDT\text{-}TTF)_2X$ [60], Mn_3CuN [61], TDAE-C_{60} [62], just to cite some examples. This implies that, indeed, the known universality classes do not cover the whole spectrum of magnetism and, therefore, more theoretical work should be done in order to propose new universality classes. In this particular case, it is the presence of Tb which takes the critical exponents to such values, even if neutron diffraction data agree at 200 K with a collinear ferromagnetic state, with Tb occupying two non-equivalent positions; it is the low temperature transition which is ferromagnetic non collinear [21].

In order to check the appropriateness of the values of the critical exponents found, detailed specific heat measurements in the near vicinity of the phase transition have also been undertaken, from where the critical exponent α can be extracted, by means of fitting the experimental points to the function [63, 64]:

$$c_p = B + Ct + A^{\pm}|t|^{-\alpha}\left(1 + E^{\pm}|t|^{0.5}\right) \quad (8)$$

where t is the reduced temperature and α, $A^{\pm}$, B, C and $E^{\pm}$ are adjustable parameters. Superscripts + and – stand for $T > T_C$ and $T < T_C$ respectively.

In the particular case in which the Mean Field model is of application ($\alpha = 0$), the critical equation would take an asymptotical logarithmic form at the paramagnetic phase, while the ferromagnetic phase should be described by a Landau classical formulation. Therefore, the paramagnetic region is fitted to

$$c_p = A \ln t + B + Ct \tag{9}$$

while for the ferromagnetic one

$$c_p = A_1 \frac{T}{\sqrt{1 - 4A_2(T - T_C)}} + B' + C'(T - T_C) \tag{10}$$

[65]. The full details of this standard fitting procedure can be found elsewhere [21, 64, 65]. Fig. 10 shows c_p and the corresponding fittings for the four compounds. For Gd_6FeBi_2 the best fitting has corresponded to Eq. (8) with α = -0.075±0.007, which is close to the theoretical one for the 3D-Heisenberg model (α_{exp} = -0.115); besides, the critical ratio A^+/A^- = 1.32 while A^+/A^-_{Heis} = 1.52. Other models have been tested but none of them has given a good fitting. This corroborates the previous magnetic results, implying that the PM-FM belongs to the Heisenberg class with a certain deviation from it.

In the other three compounds, the fitting to Eq. (8) have not given good results, the best ones being obtained by using Eqs (9) and (10). Starting with $Gd_3Tb_3FeBi_2$, both phases agreed quite well with this model but not exactly, as seen in the difficulty in fitting the curvature of the paramagnetic phase (see Fig. 10b). This corroborates the magnetic exponents, which are quite close to the Mean Field model but with a slight separation from it. Tb_6FeBi_2 deviates even more from the Mean Field model (see Fig 10c), while the introduction of Mn in $Tb_6Fe_{0.5}Mn_{0.5}Bi_2$ alters the shape of the specific heat and makes quite difficult any fitting (see Fig. 10d), the best one being obtained again with Eqs (9) and (10). These results corroborate the unconventional critical behaviour of these Tb-based compounds, which will be further confirmed by the scaling of the magnetic entropy change (Eq. (5)) presented in the next section.

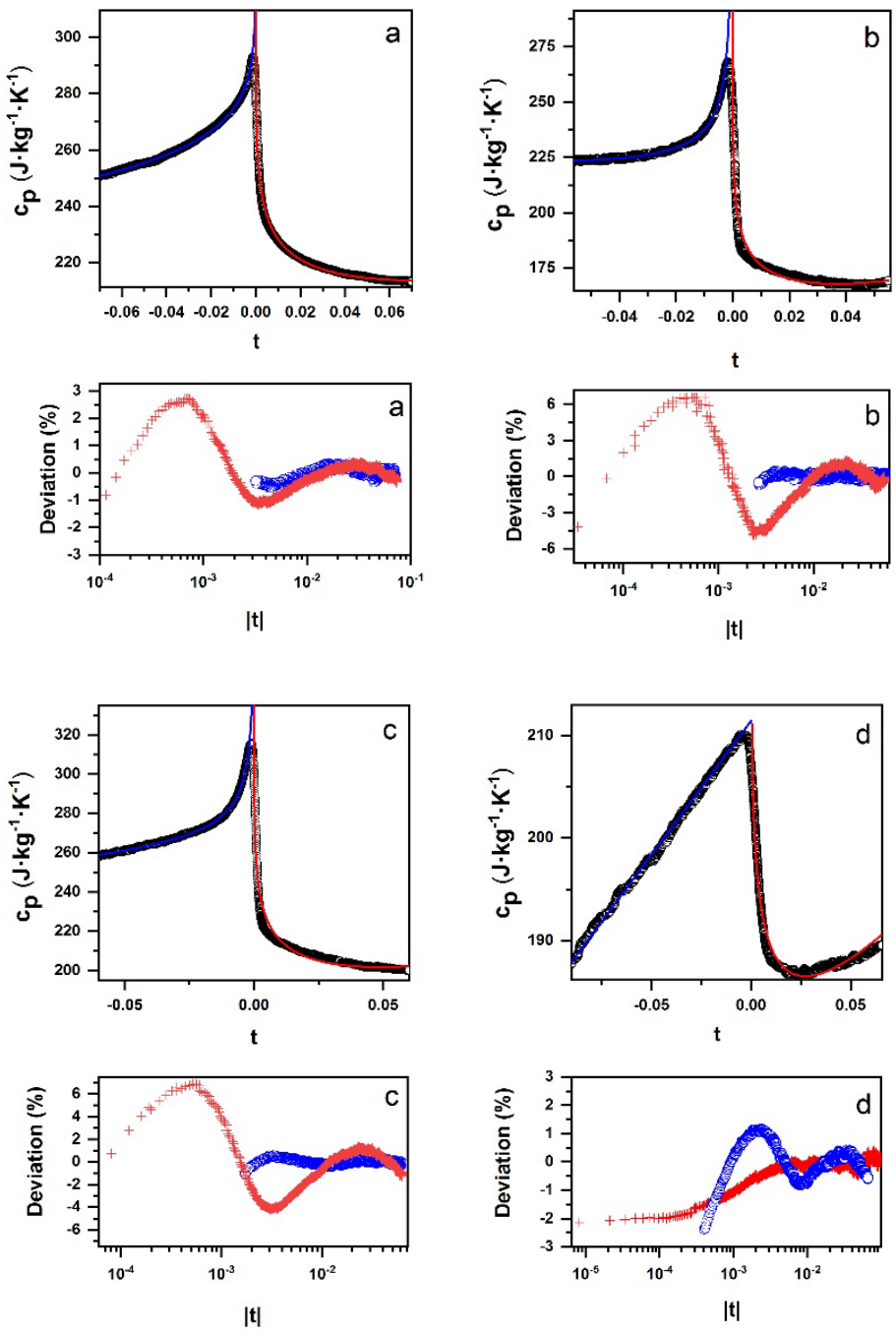

Fig. 10. Experimental (dots) and fitted curves (continuous lines) of the specific heat as a function of the reduced temperature for the four compounds in the near vicinity of T_C (top in each case); deviation plots for the fittings (bottom in each case), where open circles are for $T < T_C$, crosses for $T > T_C$. a) Gd_6FeBi_2, b) $Gd_3Tb_3FeBi_2$, c) Tb_6FeBi_2, and d) $Tb_6Fe_{0.5}Mn_{0.5}Bi_2$.

3.2 Magnetocaloric properties.

The magnetocaloric properties of these compounds have been studied by the common, indirect method, of evaluating the magnetic entropy change as a function of temperature and magnetic field

$$\Delta S_M(\mathrm{T},\Delta\mathrm{H}) = \mu_0 \int_{H_i}^{H_f} \left(\frac{\partial M}{\partial T}\right)_H dH \qquad (11)$$

The results are shown in Fig. 11 where it is seen that there is only one direct MCE for Gd_6FeBi_2, while there are two for the other three compounds, associated to the PM-FM transitions at high temperatures and to the spin reorientation transitions at low ones. The maximum values $\left|\Delta S_M^{pk}\right|$ are similar to what is obtained in many other rare-earth-based materials [2, 4, 5] but there are several additional features worth studying, specially the fact that the temperature span of the magnetocaloric effect is extended in the case where there are two magnetic transitions, giving relevant values of the refrigerant capacities *RC*.

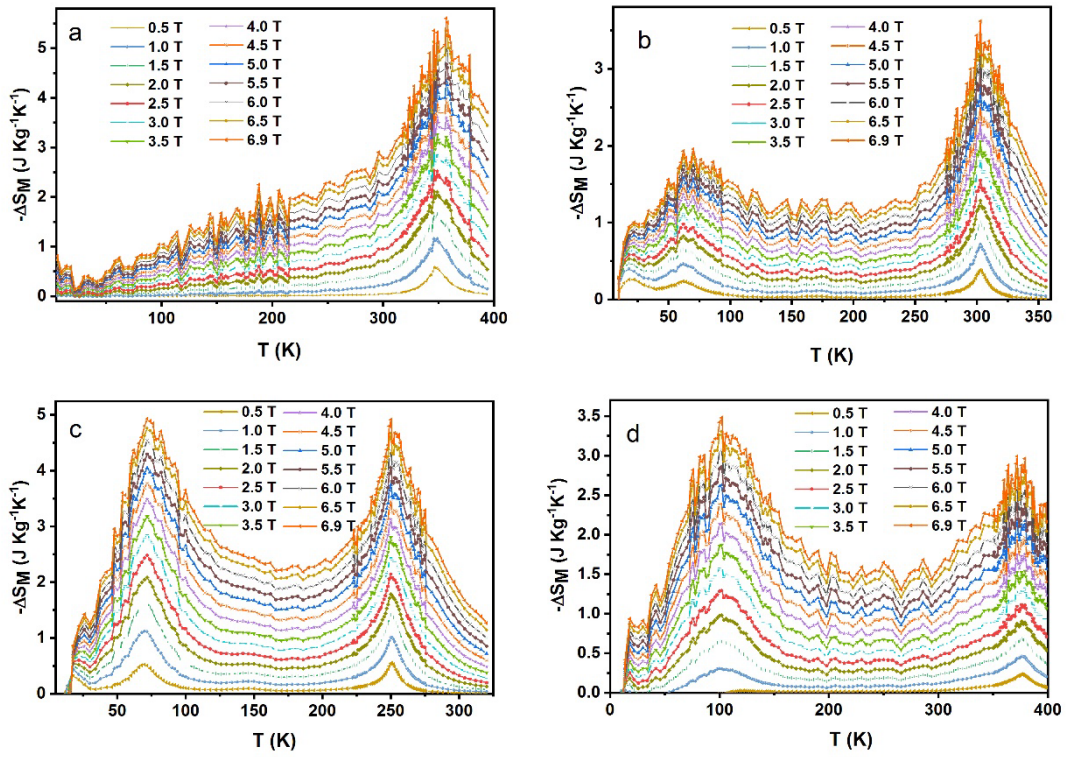

Fig. 11. Magnetic entropy change $-\Delta S_M$ for $\mu_0\Delta H$ from 1 T to 6.9 T for: a) Gd_6FeBi_2, b) $Gd_3Tb_3FeBi_2$, c) Tb_6FeBi_2, and d) $Tb_6Fe_{0.5}Mn_{0.5}Bi_2$.

In literature, *RC* is commonly defined in two ways. RC_{FWHM} is obtained multiplying the width of the magnetic entropy change at half maximum times the value of the peak,

$$RC_{FWHM} = \left|\Delta S_M^{pk}\right| \delta T_{FWHM} \quad (12)$$

while RC_{AREA} is defined as the area enclosed by the magnetic entropy change vs. temperature curve in the range enclosed by the full width at half maximum (FWHM).

$$RC_{AREA} = \int_{T_{cold}}^{T_{hot}} \Delta S_M(T, \Delta H) dT \quad (13)$$

The values of the refrigerant capacities, as well as the maxima of $\left|\Delta S_M^{pk}\right|$ are tabulated in Table 4 for $\mu_0 \Delta H$ = 2, 5 and 6.9 T, the first ones for the sake of comparison with literature, the third one being the highest field applied. As in Gd_6FeBi_2 and $Tb_6(Fe_{0.5}Mn_{0.5})Bi_2$ *Tc* is quite high and our system can not measure above 400K, some values for *RC* have had to be obtained from extrapolations, while some RC_{Area} can not be obtained (these values are clearly indicated in Table 4). Starting from Gd_6FeBi_2, codoping it with Tb ($Gd_3Tb_3FeBi_2$) takes the maximum values from 346 to 303 K (therefore approaching room temperature) though $\left|\Delta S_M^{pk}\right|$ is reduced; the appearance of the spin reorientation transition at 62 K makes the values of $\left|\Delta S_M\right|$ increase at medium temperatures. With the complete substitution of Gd by Tb, there are nearly equivalent peaks at $\mu_0 \Delta H$ = 5 T, placed at 72 and 250 K, which are both interesting regions of application, with RC_{FWHM} being 279 and 231 J/kg.K and a very wide temperature span of the magnetocaloric effect between the peaks. Finally, there is a similar effect when partially substituting Fe by Mn but displacing the maxima to 102 and 376 K and, though the maxima are smaller, the RC_{FWHM} is maintained at T_m while it increases at T_C due to the widening of the peak (279 and 266 J/kg.K, respectively).

These results show, on the one hand, the interest in mixing Gd and Tb (Fig. 11a, b, c) in order to tune the region of application and, on the other, to substitute Fe by Mn in the Tb-based compounds, to even enhance the effect (Fig. 11d). The results here obtained are comparable to previously published results on the value of $\left|\Delta S_M^{pk}\right|$ at T_C for Gd_6FeBi_2 [24] and Tb_6FeBi_2 [22], though they had not been studied in the full temperature range. If we compare them with other rare-earth based compounds, the values of $\left|\Delta S_M^{pk}\right|$ are not too high (for instance, compared to the results presented in Fig. 25 of ref. [2]) though the refrigerant capacity and temperature span are fully competitive [2, 4, 5].

The magnetocaloric effect also gives the possibility of studying the critical behaviour of the PM-FM transition, as it follows from Eq. (5) that it scales with the critical exponent *n*, which is a combination of β and δ. With the values of the critical exponents

calculated in the previous section, we have calculated n and Fig. 12 represents the scaling function for Gd_6FeBi_2 and Tb_6FeBi_2, where it is clearly seen that there is a very good agreement, as the experimental points lie, in all cases, along the straight line, confirming the validity of the critical exponents. For the other compounds, the agreement is as good as in Fig. 12.

Moreover, the refrigerant capacity also scales as

$$RC \propto H^{1+1/\delta}, \tag{14}$$

Fig. 13 shows the experimental RC_{FWHM} as a function of $H^{1+1/\delta}$ using the value of delta obtained from the critical isotherms for $Gd_3Tb_3FeBi_2$ and $Tb_6Fe_{0.5}Mn_{0.5}Bi_2$, where the theoretical line is also traced. Again, the experimental points lie extremely well along the straight line.

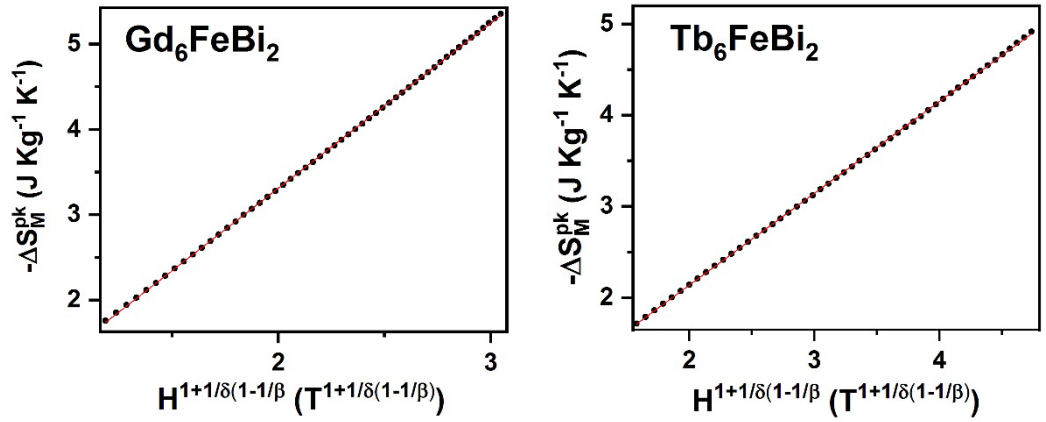

Fig. 12. Field dependences of the peak magnetic entropy change for Gd_6FeBi_2 (left) Tb_6FeBi_2 (right). The values of β and δ for each compound are the ones presented in Table 3.

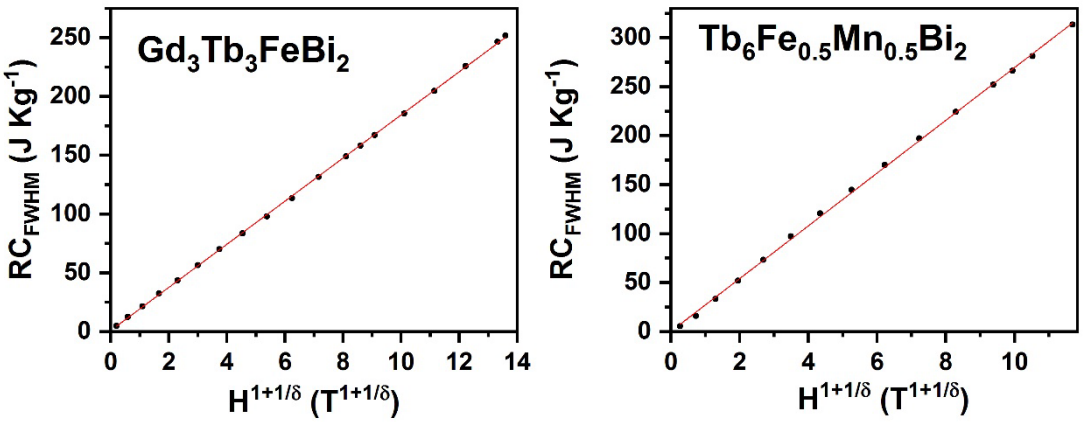

Fig. 13. Scaling law for the refrigerant capacity RC_{FWHM} for $Gd_3Tb_3FeBi_2$ (a) and $Tb_6Fe_{0.5}Mn_{0.5}Bi_2$ (b). The values of δ for each compound are the ones presented in Table 3.

Besides, it should be feasible to build up universal curves for each compound around T_C [27]; the method consists on normalizing the variation of the magnetic entropy change for each field with respect to the corresponding maximum value and rescaling the temperature axis. In an ideal case, only one reference temperature T_r is needed in order to obtain a good universal curve, scaling the temperature axis as follows:

$$\theta_1 = \frac{T - T_C}{T_r - T_C}. \tag{15}$$

T_r is selected to be above T_C, corresponding to a particular fraction of $\left|\Delta S_M^{pk}\right|$, which has been 0.5. Nevertheless, when there are additional effects, such as the presence of additional magnetic phases or demagnetization effects, two reference temperatures T_{r1}, T_{r2} are needed to develop the universal curves [28]. This happens, in particular, when demagnetization effects are not negligible, as it happens in this case:

$$\theta_2 = \begin{cases} -(T - T_C)/(T_{r1} - T_C) & , \quad T \le T_C \\ (T - T_C)/(T_{r2} - T_C) & , \quad T > T_C \end{cases} \tag{16}$$

Fig. 14 shows the universal curves using one and two reference temperatures for $Gd_3Tb_3FeBi_2$. The overlapping must take place in the critical region, i.e., in the near vicinity of the second order phase transition [29, 66], where critical theory is fulfilled. It is clear that this happens in both cases, much better with two reference temperatures. In the one with one reference, the curves just below T_C do not perfectly overlap but they move to higher values of $\frac{\Delta S_M}{\Delta S_M^{pk}}$ as the magnetic field increases, typical of systems where demagnetization effects are present [67], as it is the case. When using two reference temperatures this effect disappears, confirming the theory. At temperatures far below T_C, the curves spread out and the values quickly increase, what happens in the three compounds where there is a spin reorientation transition at a low temperature. If in the region in which this methodology is applied there is another magnetic transition, no good overlapping is expected where this second transition is present, as the theory is based on the fact that the PM-FM transition belongs to a particular universality class, which is the case here. The universal curve is similarly built up for the four compounds.

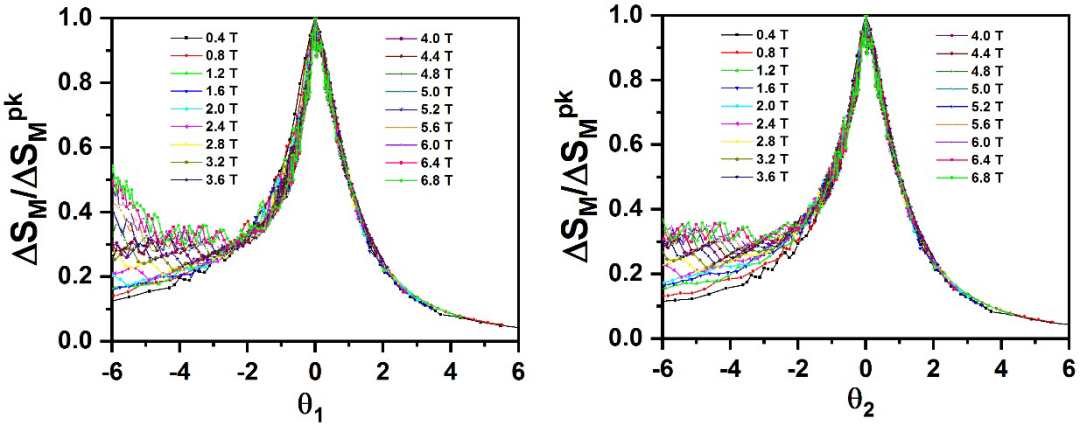

Fig. 14. Universal curve with the rescaled magnetic entropy changes using one (left) or two (right) reference temperatures, for $Gd_3Tb_3FeBi_2$.

The importance of the scaling of the magnetocaloric variables ($\left|\Delta S_M^{pk}\right|$ and RC) is that it allows their extrapolation to different fields, even if they have not been measured, while the universal curves allows the extrapolation of the whole magnetic entropy change curves to no accessible magnetic fields [66].

A final interesting remark has to do with the magnetocaloric effect at very low temperature, which has not been shown in Fig. 11. Due to the magnetic behaviour shown in this range by $Gd_3Tb_3FeBi_2$, Tb_6FeBi_2, and $Tb_6Fe_{0.5}Mn_{0.5}Bi_2$, an inverse magnetocaloric effect (IMCE) is expected. As there are metamagnetic transitions in this range, whose first order is clearly observed due to the stepwise behavior (see Fig. 4), the calculation of the magnetic entropy change can only be accomplished using Eq. (11) if the measurement of each magnetization isotherm is taken after having erased the magnetic memory of the sample, or a spurious result would be obtained [68, 69]. Following this procedure, previously to obtain any magnetization isotherm as a function of the applied field, the temperature is raised, without field, above T_C. Then the temperature is taken to the one corresponding to the next isotherm and the field is applied again. The procedure is repeated isotherm after isotherm. A huge IMCE has been found in this way in $Gd_3Tb_3FeBi_2$, extremely narrow, centered at T' = 3 K (see Fig. 15), with ΔS_M^{pk} = 36.5 J/kg.K at $\mu_0\Delta H$ = 5 T and RC_{FWHM} = 46 J/kg, RC_{Area} = 34 J/kg. A relevant IMCE is also found for Tb_6FeBi_2, which becomes a wide plateau as $\mu_0\Delta H$ is increased, centered around T' = 7 K. The maximum value ΔS_M^{pk} is smaller than in the previous case (16.5 J/kg.K at $\mu_0\Delta H$ = 5 T) but the refrigerant capacity is significantly higher (RC_{FWHM} = 137 J/kg, RC_{Area} = 118 J/kg). Finally, for the case of $Tb_6Fe_{0.5}Mn_{0.5}Bi_2$, the IMCE is less significant, with

a broad peak with maximum at T' = 4.5 K, ΔS_M^{pk} = 13.1 J/kg.K, RC_{FWHM} = 70 J/kg, RC_{Area} = 53 J/kg, all at $\mu_0 \Delta H$ = 5 T; this compound presents another DMCE at very low temperature due to the magnetic properties already shown in Fig. 5. Table 5 contains all these results together with the ones at $\mu_0 \Delta H$ = 2 and 6.9 T, for the sake of comparison.

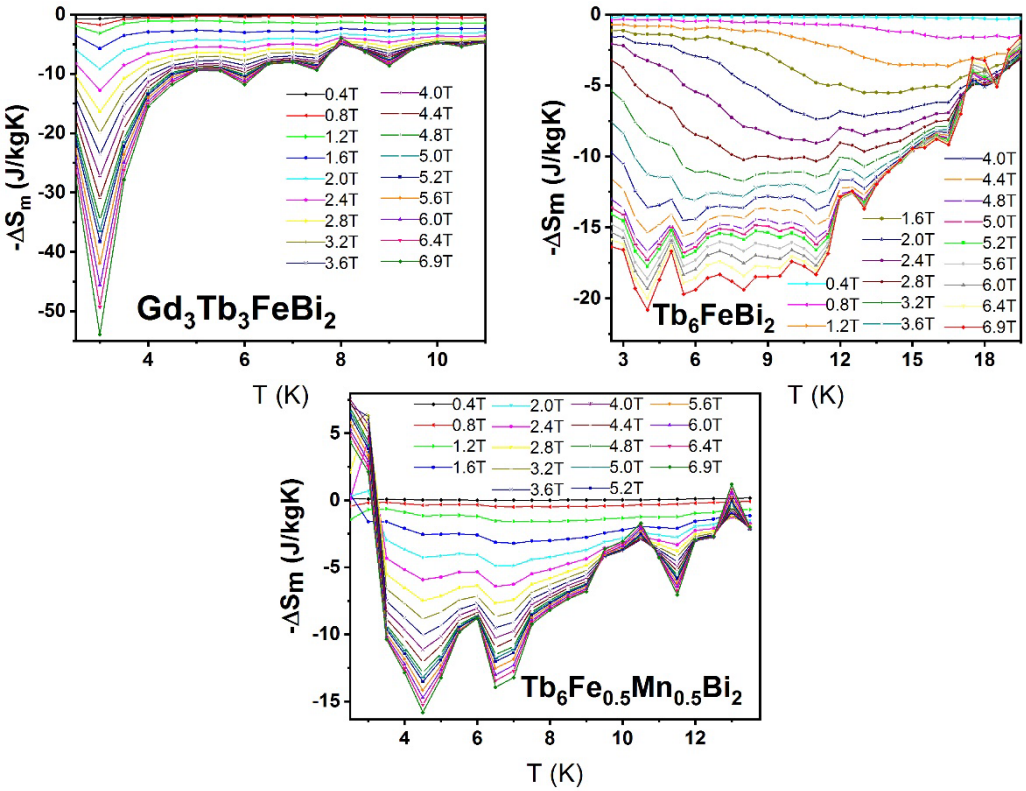

Fig. 15. Magnetic entropy change $-\Delta S_M$ for $\mu_0 \Delta H$ from 1 T to 6.9 T, at very low temperature, showing the inverse magnetocaloric effect (IMCE): a) $Gd_3Tb_3FeBi_2$, b) Tb_6FeBi_2, and c) $Tb_6Fe_{0.5}Mn_{0.5}Bi_2$.

Materials with an IMCE can be, of course, used as coolers, but also as heat-sinks for heat generated when a conventional magnetocaloric material is magnetized before cooling by adiabatic demagnetization [12, 70]; in this particular application, materials with adjoint IMCE and DMCE, as is the case, can increase the refrigeration efficiency [71, 72].

4. Conclusions

Rare earth as well as transition metal substitution in the intermetallic family $(Gd,Tb)_6(Fe,Mn)Bi_2$ brings interesting changes in their magnetic properties which allow to tune the magnetocaloric properties in a wide temperature range, including room temperature, and broaden their applications as adjoint direct and inverse MCE can be obtained. The substitution of Gd by Tb (Gd_6FeBi_2, $Gd_3Tb_3FeBi_2$, Tb_6FeBi_2) tunes T_C,

taking it from 346 K to 303 K, and then to 250 K, favoring the apparition of a spin reorientation transition at T_m = 62 and 72 K ($Gd_3Tb_3FeBi_2$ and Tb_6FeBi_2, respectively) as well as a metamagnetic transition at very low temperature from a complex non-collinear magnetic state to a ferromagnetic state. Therefore, an inverse magnetocaloric effect (IMCE) appears with a maximum at T' = 3K, ΔS_M^{pk} = 36.5 J/kg.K, RC_{FWHM} = 46 J/kg (at $\mu_0 \Delta H$ = 5 T) for $Gd_3Tb_3FeBi_2$ and at T' = 7 K, ΔS_M^{pk} = 16.5 J/kg.K, RC_{FWHM} = 137 J/kg (for $\mu_0 \Delta H$ = 5 T) for Tb_6FeBi_2. In both Tb-containing samples, a direct magnetocaloric effect (tableau-shaped) appears over a wide temperature span between T_C and T_m with maxima at those temperatures. The partial substitution of Fe by Mn in $Tb_6Fe_{0.5}Mn_{0.5}Bi_2$ shifts these effects upwards in temperature while expanding the region of the direct magnetocaloric effect between 70 and 400 K. Besides, the critical behavior of the PM-FM transitions has been studied obtaining the critical exponents $\alpha, \beta, \gamma, \delta$ which agree with the scaling of the magnetocaloric variables ΔS_M^{pk} and RC_{FWHM}, having obtained universal curves for the magnetocaloric effect in all cases. The transition in Gd_6FeBi_2 has been found to belong to the Heisenberg universality class with deviations due to magnetocrystalline anisotropies; the one in $Gd_3Tb_3FeBi_2$ to the Mean Field class, implying that short range order interactions have given way to long range ones, while Tb_6FeBi_2 and $Tb_6Fe_{0.5}Mn_{0.5}Bi_2$ present an unconventional critical behavior aligned with long range order interactions.

Acknowledgements

This work has been supported by Universidad del País Vasco UPV/EHU (project GIU19/305) and the Russian Fund for Basic Research (project N° 20-03-00209-a). A. Herrero thanks the Department of Education of the Basque Government as grantee of the programme "Programa Predoctoral de Formación de Personal Investigador No Doctor". The authors thank for technical and human support provided by SGIker of UPV/EHU.

Appendix A. Supplementary Material

Supplementary data to this article can be found at the end of the text

References

[1] A.M. Tishin, Y.I. Spichkin, *The Magnetocaloric Effect and its Applications*, Series in Condensed Matter Physics, Institute of Physics Publishing, Bristol and Philadelphia (2003).

[2] V. Franco, J.S. Blázquez, J.J. Ipus, J.Y. Law, L.M. Moreno-Ramírez, A. Conde, *Magnetocaloric effect: From materials research to refrigeration devices*, Prog. Mat. Sci. 93 (2018) 112-232.

[3] T. Gotschall, K.P. Skokov, M. Fries, A. Taubel, I. Radulov, F. Scheibel, D. Benke, S. Riegg, O. Gutfleisch, *Making a cool choice: The materials library of magnetic refrigeration*, Adv. Energy Mater. 9 (2019) 1901322 (1-13).

[4] Y. Zhang, *Review of the structural, magnetic and magnetocaloric properties in ternary rare earth RE_2T_2X type intermetallic compounds*, J. Alloys Compd. 787 (2019) 1173-1186.

[5] H. Zhang, R. Gimaev, B. Kovalev, K. Kamilov, V. Zverev, *Review on the materials and devices for magnetic refrigeration in the temperature range of nitrogen and hydrogen liquefaction*, Phys. B: Condens. Matter 558 (2019) 65-73.

[6] L.W. Li, *Review of magnetic properties and magnetocaloric effect in the intermetallic compounds of rare earth with low boiling point*, Chin. Phys. B 25 (2016) 037502.

[7] K.A. Gschneidner Jr, V.K. Pecharsky, A.O. Tsokol, *Recent developments in magnetocaloric materials*, Rep. Prog. Phys. 68 (2005) 1479-1539.

[8] L. Li, M. Yan, *Recent progresses in exploring the rare earth based intermetallic compounds for cryogenic magnetic refrigeration*, J. Alloys Compd. 823 (2020) 153810.

[9] V.K. Pecharsky, K.A. Gschneider Jr., *Giant magnetocaloric effect in $Gd_5Si_2Ge_2$,* Phys. Rev. Lett. 78 (1997) 4494-4497.

[10] S. Couillaud, E. Gaudin, V. Franco. A. Conde, R. Pöttgen, B. Heying, U.Ch. Rodewald, B. Chevalier, *The magnetocaloric properties of GdScSi and GdScGe*, Intermetallics 19 (2011) 1573-1578.

[11] A. Herrero, A. Oleaga, P. Manfrinetti, A. Provino, A Salazar, *Study of the magnetocaloric effect in intermetallics RTX (R = Nd, Gd; T = Sc, Ti ; X = Si, Ge)*, Intermetallics 110 (2019) 106495.

[12] T. Krenke, E. Duman, M. Acet, E.F. Wassermann, X. Moya, L. Mañosa, A. Planes, *Inverse magnetocaloric effect in ferromagnetic Ni-Mn-Sn alloys*, Nat. Mater. 4 (2005) 450-454.

[13] F. Hu, B. Shen, J. Sun, *Magnetic entropy change in $Ni_{51.5}Mn_{22.7}Ga_{25.8}$ alloy*, Appl. Phys. Lett. 76 (2000) 3460-3462.

[14] Z.B. Guo, Y.W. Du, J.S. Zhu, H. Huang, W.P. Ding, D, Feng, *Large magnetic entropy change in perovskite-type manganese oxides*, Phys. Rev. Lett. 78 (1997) 1142-1145.

[15] A. Fujita, S. Fujieda, Y. Hasegawa, K. Fukamichi, *Intinerant-electron metamagnetic transition and large magnetocaloric effects in $La(Fe_xSi_{1-x})_{13}$ compounds and their hydrides*, Phys. Rev. B 67 (2003) 104416.

[16] H. Wada, Y. Tanabe, *Giant magnetocaloric effect of $MnAs_{1-x}Sb_x$*, Appl. Phys. Lett. 79 (2001) 3302-3304.

[17] F. Chen, J.L. Sanchez Llamazares, C.F. Sanchez-Valdes, F. Chen, Z. Li, Y.X. Tong, L. Li, *Large magnetic entropy change and refrigeration capacity around room temperature in quinary Ni41Co9-xFexMn40Sn10 alloys (x¼ 2.0 and 2.5)*, J. Alloys Compd. 825 (2020) 154053.

[18] H. Zhang, Y.J. Sun, E. Niu, L.H. Yang, J. Shen, F.X. Hu, J.R. Sun, B.G. Shen, *Large magnetocaloric effects of RFeSi (R = Tb and Dy) compounds for magnetic refrigeration in nitrogen and natural gas liquefaction*, Appl. Phys. Lett. 103 (2013) 202412.

[19] A. Herrero, A. Oleaga, A. Salazar, A.V. Garshev, V.O. Yapaskurt, A.V. Morozkin, *Magnetocaloric properties, magnetic interactions and critical behavior in $Ho_6(Fe,Mn)Bi_2$ intermetallics*, J. Alloys Compd. 821 (2020) 153198.

[20] A.V. Morozkin, *New Zr_6CoAs_2-type R_6FeBi_2 (R=Y, Lu, Gd-Dy, Er, Tm)*, J. Alloys Compd. 358 (2003) L9-L10.

[21] A.V. Morozkin, V.N. Nikiforov, B. Malaman, *Magnetic structure of the Zr_6CoAs_2-type Tb_6FeBi_2 compound,* J. Alloys Compd. 393 (2005) L6-L9.

[22] W. He, J. Zhang, L. Zeng, P. Qin, G. Cai, *Thermomagnetic properties near transitions of Tb_6FeX_2 (X=Sb, Bi)*, J. Alloys Compd. 443 (2007) 15-19.

[23] L. Jia, M. Koehler, D. McCarthy, M.A. McGuire, V. Keepens, *Structural and magnetic properties of $Tb_6Fe_{1-x}Co_xBi_2$ ($0 \leq x \leq 0.375$) compounds*, J. Appl. Phys. 109 (2011) 07E331.

[24] J. Zhang, G. Shan, Z. Zheng, C.H. Shek, *Structure and magnetic behaviors of Gd_6FeBi_2 compound*, Intermetallics 68 (2016) 51-56.

[25] J. Zhang, Y.M. Kang, G. Shan, S. Bobev, *Structural analysis of Gd_6FeBi_2 from single-crystal X-ray diffraction methods and electronic structure calculations*, Acta Crystallogr. C 75 (2019) 562-567.

[26] G. Cuia, H. Mab, K. W. Wongc, C. H. S., G. Shand, J. Zhange, *Understanding high ordering temperature in Gd6FeBi2 magnet: Critical behavior, electronic structure and crystal-field analysis*, J. Magn. Magn. Mater. 499 (2020) 166301.

[27] V. Franco, A. Conde, J.M. Romero-Enrique, J.S. Blázquez, *A universal curve for the magnetocaloric effect: an analysis based on scaling relations,* J. Phys.: Condens. Matter 20 (2008) 285207 (5pp).

[28] V. Franco, J.S. Blázquez, A. Conde, *Field dependence of the magnetocaloric effect in materials with a second order phase transition: A master curve for the magnetic entropy change*, Appl. Phys. Lett. 89 (2006) 222512.

[29] C. Romero-Muñiz, R. Tamura, S. Tanaka, V. Franco, *Applicability of scaling behavior and power laws in the analysis of the magnetocaloric effect in second-order phase transition materials*, Phys. Rev. B 94 (2016) 134401.

[30] H.E. Stanley, *Introduction to phase transitions and critical phenomena*, Oxford University Press (1971).

[31] F. Izumi, in: R.A. Young (Ed.), *The Rietveld Method*, Oxford University Press, Oxford, 1993, Chap. 13.

[32] H. Neves Bez, H. Yibole, A. Pathak, Y. Mudryk, V.K. Pecharsky, *Best practices in evaluation of the magnetocaloric effect from bulk magnetization measurements,* J. Magn. Magn. Mater. 458 (2018) 301–309.

[33] A.M. Tishin, *A review and new perspectives of the magnetocaloric effect: New materials and local heating and cooling inside the human body*, Int. J. Refrig. 68 (2016) 177-186.

[34] W. Jiang, X.Z. Zhou, G. Williams, Y. Mukovskii, K. Glazyrin, *Magnetic ground state and two-dimensional behavior in pseudo-kagome layered system* $Cu_3Bi(SeO_3)_2O_2Br$, Phys. Rev. B 78 (2008) 144409.

[35] W. Jiang, X.Z. Zhou, G. Williams, Y. Mukovskii, K. Glazyrin, *Coexistence of colossal magnetoresistance, a Griffiths-like phase, and a ferromagnetic insulating ground state in single crystal* $La_{0.73}Ba_{0.27}MnO_3$, Phys. Rev. B 77 (2008) 064424.

[36] U. Zammit, S. Paoloni, F. Mercuri, M. Marinelli, F. Scudieri, *Photopyroelectric calorimeter for the simultaneous thermal, optical, and structural characterization of samples over phase transitions*, AIP Advances 2 (2012) 012135.

[37] A. Oleaga, A. Salazar, D. Prabhakaran, J.G. Cheng, J.S. Zhou, *Critical behavior of the paramagnetic to antiferromagnetic transition in orthorhombic and hexagonal phases of* $RMnO_3$ *(R = Sm, Tb, Dy, Ho, Er, Tm, Yb, Lu, Y)*, Phys. Rev. B 85 (2012) 184425.

[38] M. Massot, A. Oleaga, A. Salazar, D. Prabhakaran, M. Martin, P. Berthet, G. Dhalenne, *Critical behavior of CoO and NiO from specific heat, thermal conductivity, and thermal diffusivity measurements*, Phys. Rev. B 77 (2008) 134438.

[39] A.V. Morozkin, R. Nirmala, S.K. Malik, *Structural and magnetic properties of Fe_2P-type R_6TX_2 compounds (R = Zr, Dy, Ho, Er, Tj Mn, Fe, Co, Cu, Ru, Rh, X = Sb, Bi, Te)*, Intermetallics 19 (2011) 1250-1264.

[40] J. Szade, M. Drzyzga, *Magnetism and electronic structure of Gd_5Bi_3 and Gd_4Bi_3*, J. Alloys Compd. 299 (2000) 72–78.

[41] S. Legvold, in Rare Earth Metals and Alloys, Ferromagnetic Materials (E.P. Wohlfarth, Edit.), Amsterdam, North-Holland Publish. Comp. (1980) 183-295.

[42] A.V. Morozkin, O. Isnard, P. Manfrinetti, A. Provino, C. Ritter, R. Nirmala, S.K. Malik, *The magnetic ordering in the Ho_6FeTe_2*, J. Alloys Compd. 498 (2010) 13-18.

[43] A.V. Morozkin, YuMozharivskyj, V.Svitlyk, R.Nirmala, O.Isnard, P.Manfrinetti, A. Provino, C.Ritter, *Magnetic properties of Fe_2P-type R_6CoTe_2 compounds (R=Gd–Er)*, J. Solid State Chem. 183 (2010) 1314-1325.

[44] A.K. Pramanik, A. Banerjee, *Critical behavior at paramagnetic to ferromagnetic phase transition in $Pr_{0.5}Sr_{0.5}MnO_3$: A bulk magnetization study*, Phys. Rev. B 79 (2009) 214426.

[45] A. Oleaga, A. Salazar, M. Ciomaga Hatnean, G. Balakrishnan, *Three-dimensional Ising critical behavior in $R_{0.6}Sr_{0.4}MnO_3$(R=Pr,Nd) manganites*, Phys. Rev. B 92 (2015) 024409.

[46] A.V. Morozkin, R. Nirmala, S.K. Malik, *Magnetic structure of the Zr_6CoAs_2-type Er_6TX_2 compounds (T= Mn, Fe, Co and X=Sb, Bi)*, J. Alloys Compd. 394 (2005) 75-79.

[47] S.N. Kaul, S. Srinath, *Gadolinium: A helical antiferromagnet or a collinear ferromagnet*, Phys. Rev. B 62 (2000) 1114.

[48] S. Gupta, K.G. Suresh, *Review on magnetic and related properties of RTX compounds*, J. Alloys Compd. 618 (2015) 562-606.

[49] G. Bednarz, D.J.W. Geldart, M.A. White, *Heat capacity of gadolinium near the Curie temperature*, Phys. Rev. B 47 (1993) 14247.

[50] C. Glorieux, J. Thoen, G. Bednarz, M.A. White, D.J.W. Geldart, *Photoacoustic investigation of the temperature and magnetic-field dependence of the specific-heat capacity and thermal conductivity near the Curie point of gadolinium*, Phys. Rev. B 52 (1995) 12770.

[51] A. Herrero, A. Oleaga, P. Manfrinetti, A. Provino, A. Salazar, *Critical behavior of the ferromagnetic transition in GdSc(Si,Ge) intermetallic compounds*, Intermetallics 101 (2018) 64–71.

[52] M. Colarieti-Tosti, T. Burkert, O. Eriksson, L. Nordström, M.S.S. Brooks, *Theory of the temperature dependence of the easy axis of magnetization in hcp Gd*, Phys. Rev. B 72 (2005) 094423.

[53] F. Guillou, A.K. Pathak, T.A Hackett, D. Paudyal, Y. Mudryk, V.K. Pecharsky, *Crystal, magnetic, calorimetric and electronic structure investigation of $GdScGe_{1-x}Sb_x$ compounds*, J. Phys.: Condens. Matter 29 (2017) 485802.

[54] D.A Shishkin, A.S. Volegov, V.V. Obloblichev, K.N. Mikhalev, E.G. Gerasimov, P.B. Terentev, V.S. Gaviko, D.I. Gorbunov, N.V. Baranov, *Effect of Tb for Gd substitution ion magnetic and magnetocaloric properties of melt-spun $(Gd_{1-x}Tb_x)_3Co$ alloys*, Intermetallics 104 (2019) 1-7.

[55] Y. Itoh, T. Mizoguchi, K. Yoshimura, *Novel critical exponent of magnetization curves near the ferromagnetic quantum phase transitions of $Sr_{1-x}Ca_xRuO_3$ (A=Ca, $La_{0.5}Na_{0.5}$, and La)*, J. Phys. Soc. Jpn. 77 (2008) 123702.

[56] D. Fuchs, M. Wissinger, J. Schmalian, C.-L. Huang, R. Fromknecht, R. Schneider, H. v. Löhneysen, *Critical scaling analysis of the itinerant ferromagnet $Sr_{1-x}Ca_xRuO_3$*, Phys. Rev. B 89 (2014) 174405.

[57] N. Assoudi, M. Smari, I. Walha, E. Dhahri, S. Shevyrtalov, O. Dikaya, V. Rodionova, *Unconventional critical behavior near the phase transition temperature and magnetocaloric effect in $La_{0.5}Ca_{0.4}Ag_{0.1}MnO_3$ compound*, Chem. Phys. Lett. 706 (2018) 182-188.

[58] M. Triki, E. Dhahri, E.K. Hlil, *Unconventional critical magnetic behaviour in the Griffiths ferromagnet $La_{0.4}Ca_{0.6}MnO_{2.8}$ $\square_{0.2}$ oxide*, J. Sol. State Chem. 201 (2013) 63-67.

[59] T. Kida, A. Senda, S. Yoshii, M. Hagiwara, T. Takeuchi, T. Nakano, I. Terasaki, *Unconventional critical behaviour in the weak ferromagnet $BaIrO_3$*, EPL 84 (2008) 27004.

[60] F. Kagawa, K. Miyagawa, K. Kanoda, *Unconventional critical behaviour in a quasi-two-dimensional organic conductor*, Nature 436 (2005) 534.

[61] Y. Yin, J.C. Han. Q. Yuan, L.S. Ling, B. Song, *Critical behaviour in the antiperovskite Mn_3CuN at ferromagnetic to paramagnetic phase transition*, J. Magn. Magn. Mater. 346 (2013) 203-208.

[62] A. Omerzu, M. Tokumoto, B. Tadić, D. Mihailovic, *Critical Exponents at the Ferromagnetic Transition in Tetrakis(dimethylamino)ethylene-C_{60} (TDAE-C_{60})*, Phys. Rev. Lett. 87 (2001) 177025.

[63] M. Marinelli, F. Mercuri, U. Zammit, R. Pizzoferrato, F. Scudieri, D. Dadarlat, *Photopyroelectric study of specific heat, thermal conductivity, and thermal diffusivity of Cr_2O_3 at the Néel transition*, Phys. Rev. B 49 (1994) 9523.

[64] A. Oleaga, A. Salazar, Yu.M. Bunkov, *3D-XY critical behaviour of $CsMnF_3$ from static and dynamic thermal properties*, J. Phys.: Condens. Matter 26 (2014) 096001.

[65] A. Oleaga, V. Liubachko, P. Manfrinetti, A. Provino, Yu. Vysochanskii, A. Salazar, *Critical behavior study of NdScSi, NdScGe intermetallic Compounds*, J. Alloys Compd. 723 (2017) 559-566.

[66] V. Franco, A. Conde, *Scaling laws for the magnetocaloric effect in second order phase transitions: From physics to applications for the characterization of materials*, Int. J. Refrig. 33 (2010) 465-473.

[67] R. Caballero-Flores, V. Franco, A. Conde, L.F. Kiss, *Influence of the demagnetizing field on the determination of the magnetocaloric effect from magnetization curves*, J. Appl. Phys. 105 (2009) 07A919.

[68] V. Franco, *Determination of the Magnetic Entropy Change from Magnetic Measurements: the Importance of the Measurement Protocol*, (2014) (http://www.lakeshore.com/products/Vibrating-Sample-Magnetometer/Pages/MCE.aspx)

[69] V. Franco, J.Y. Law, A. Conde, V. Brabander, D.Y. Karpenkov, I. Radulov, K. Skokov, O. Gutfleisch, *Predicting the tricritical point composition of a series of LaFeSi magnetocaloric alloys via universal scaling*, J. Phys. D: Appl. Phys. 50 (2017) 414004.

[70] A. Biswas, T. Samanta, S. Banerjee, I. Das, *Inverse magnetocaloric effect in polycrystalline $La_{0.125}Ca_{0.875}MnO_3$*, J. Phys. Condens. Matter 21 (2009) 506005 (3 pp).

[71] L.V.B. Diop, O. Isnard, *Inverse and normal magnetocaloric effects in $LaFe_{12}B_6$*, J. Appl. Phys. 119 (2016) 213904.

[72] J.Y. Law, V. Franco, A. Conde, S.J. Skinner, S.S. Pramana, *Modification of the order of the magnetic phase transition in cobaltites without changing their crystal space group*, J. Alloys Compd. 777 (2019) 1080-1086.

Table 1. Unit cell data of Fe_2P-type $(Gd,Tb)_6(Fe,Mn)Bi_2$ compounds [a-] (space group $P\bar{6}2m$, No. 189, *hP*9).

N	Compound	*a* (nm)	*c* (nm)	*c*/*a*	*V* (nm^3)	x_{R1}	x_{R2}	R_F (%)
1	Gd_6FeBi_2	0.83573(8)	0.42344(3)	0.50667	0.25613	0.5958(7)	0.2409(6)	4.9
2	$Gd_3Tb_3FeBi_2$	0.83233(6)	0.42198(3)	0.50699	0.25317	0.6028(6)	0.2381(5)	4.3
3	Tb_6FeBi_2	0.82913(5)	0.42050(2)	0.50716	0.25035	0.6033(6)	0.2395(6)	4.6
4	$Tb_6Fe_{0.5}Mn_{0.5}Bi_2$	0.82838(6)	0.42473(2)	0.51272	0.25241	0.5988(7)	0.2393(6)	5.6

[a-] *R*1 (3*g*) [x_{R1}, 0, 1/2], *R*2 (3*f*) [x_{R2}, 0, 0], $Mn_{1-x}Fe_x$ (1*b*) [0, 0, 1/2], Bi (2*c*) [1/3, 2/3, 0].

Table 2. Critical exponents and parameters for the most relevant universality classes

Universality class	α	β	γ	δ	*n*	A^+/A^-
Mean-field Model	0	0.5	1.0	3.0	0.666	-
3D-Ising	0.11	0.3265	1.237	4.79	0.569	0.53
3D-Heisenberg	-0.115	0.365	1.386	4.80	0.638	1.52

Table 3. Critical exponents obtained for all compounds.

Material	Technique	β	γ	δ
Gd_6FeBi_2	Modified Arrott Plot	0.369±0.004	1.188±0.007	4.22[a] ± 0.05
	Critical Isotherm			4.277 ± 0.005
$Gd_3Tb_3FeBi_2$	Modified Arrott Plot	0.58±0.02	1.01±0.02	2.8 [a] ± 0.1
	Critical Isotherm			2.618 ± 0.004
Tb_6FeBi_2	Modified Arrott Plot	0.73±0.09	0.80±0.03	2.1[a] ± 0.2
	Critical Isotherm			2.087 ± 0.001
$Tb_6(Fe_{0.5}Mn_{0.5})Bi_2$	Modified Arrott Plot	0.72±0.02	0.95±0.01	2.31 [a] ± 0.06
	Critical Isotherm			2.251 ± 0.004

[a] Calculated from Eq. (7) $\delta = 1 + \gamma/\beta$.

Table 4. Magnitude of the magnetic entropy change $\left|\Delta S_M^{pk}\right|$ and refrigerant capacities RC_{FWHM} , RC_{AREA} at different applied fields $\mu_0\Delta H$ (2, 5 and 6.9 T) for the four compounds. The indicated temperatures correspond to the position of the maximum of $-\Delta S_M$.

		Material			
		Gd_6FeBi_2	**$Gd_3Tb_3FeBi_2$**	**Tb_6FeBi_2**	**$Tb_6(Fe_{0.5}Mn_{0.5})Bi_2$**
		T_C = 346 K	**T_m = 62 K, T_C = 303 K**	**T_m = 72 K, T_C = 250 K**	**T_m = 102 K, T_C = 376 K**
2 T	$\left\|\Delta S_M^{pk}\right\|$ **(J kg^{-1} K^{-1}) [T_m]**	--	0.8	2.1	1.0
	RC_{FWHM} **(J kg^{-1}) [T_m]**	--	--	91	72
	RC_{Area} **(J kg^{-1}) [T_m]**	--	--	69	55

	$\left\|\Delta S_M^{pk}\right\|$ **(J kg^{-1} K^{-1}) [T_C]**	2.1	1.3	1.8	0.9
	***RC$_{FWHM}$* (J kg^{-1}) [T_C]**	119	43	60	73 [1]
	***RC$_{Area}$* (J kg^{-1}) [T_C]**	87	31	43	--
5 T	$\left\|\Delta S_M^{pk}\right\|$ **(J kg^{-1} K^{-1}) [T_m]**	--	1.6	4.0	2.6
	***RC$_{FWHM}$* (J kg^{-1}) [T_m]**	--	--	279	279
	***RC$_{Area}$* (J kg^{-1}) [T_m]**	--	--	208	209
	$\left\|\Delta S_M^{pk}\right\|$ **(J kg^{-1} K^{-1}) [T_C]**	4.3	2.8	3.7	2.1
	***RC$_{FWHM}$* (J kg^{-1}) [T_C]**	402 [1]	158	231	266[1]
	***RC$_{Area}$* (J kg^{-1}) [T_C]**	296 [1]	112	162	--
6.9 T	$\left\|\Delta S_M^{pk}\right\|$ **(J kg^{-1} K^{-1}) [T_m]**	--	1.9	4.9	3.5
	***RC$_{FWHM}$* (J kg^{-1}) [T_m]**	--	--	481	444
	***RC$_{Area}$* (J kg^{-1}) [T_m]**	--	--	343	326
	$\left\|\Delta S_M^{pk}\right\|$ **(J kg^{-1} K^{-1}) [T_C]**	5.4	3.6	4.9	2.9
	***RC$_{FWHM}$* (J kg^{-1}) [T_C]**	--	252	376	--
	***RC$_{Area}$* (J kg^{-1}) [T_C]**	--	178	261	--

[1] Extrapolations have been needed to obtain these values

Table 5. Inverse magnetocaloric effect.

		$Gd_3Tb_3FeBi_2$	**Tb_6FeBi_2**	**$Tb_6(Fe_{0.5}Mn_{0.5})Bi_2$**
		T' = 3 K		**T' =**
2 T	$\left\|\Delta S_M^{pk}\right\|$ **(J kg^{-1} K^{-1})**	9.2	7.4 (**T' = 13 K)**	4.9 (**T' = 7 K)**
	***RC*$_{FWHM}$ (J kg^{-1})**	20	44	40
	***RC*$_{Area}$ (J kg^{-1})**	14	35	31
5 T	$\left\|\Delta S_M^{pk}\right\|$ **(J kg^{-1} K^{-1})**	36.5	16.5 (**T' = 7 K)**	13.1 (**T' = 4.5 K)**
	***RC*$_{FWHM}$ (J kg^{-1})**	46	137	70
	***RC*$_{Area}$ (J kg^{-1})**	34	118	53
6.9 T	$\left\|\Delta S_M^{pk}\right\|$ **(J kg^{-1} K^{-1})**	53.9	19.4 (**T' = 7 K)**	15.8 (**T' = 4.5 K)**
	***RC*$_{FWHM}$ (J kg^{-1})**	56	144	75
	***RC*$_{Area}$ (J kg^{-1})**	42	119	55

Supplementary Material for

Magnetocaloric properties and unconventional critical behavior in $(Gd,Tb)_6(Fe,Mn)Bi_2$ intermetallics

A. Oleaga, A. Herrero, A Salazar, A.V. Garshev, V. O. Yapaskurt, A.V. Morozkin

Table 1s. Sample's content and unit cell data of phases from X-ray powder and X-ray microprobe quantitative elemental analysis.

N	Sample	Phase [a-]	wt.%	Structure	*a* (nm)	*b* (nm)	*c* (nm)	R_F (%)
1	'Gd_6FeBi_2'	Gd_6FeBi_2	~90	Fe_2P	0.83573(8)		0.42344(3)	4.9
		$Gd_5Fe_{0.55}Bi_{2.45}$	~10	Yb_5Sb_3	1.1995(7)	0.9389(5)	0.8137(6)	5.4
2	'$Gd_3Tb_3FeBi_2$'	$Gd_3Tb_3FeBi_2$	~92	Fe_2P	0.83233(6)		0.42198(3)	4.3
		$Gd_{2.5}Tb_{2.5}Fe_{0.8}Bi_{2.2}$	~8	Yb_5Sb_3	1.2111(6)	0.9220(6)	0.8059(4)	4.4
3	'Tb_6FeBi_2'	Tb_6FeBi_2	~90	Fe_2P	0.82913(5)		0.42050(2)	4.6
		$Tb_5Fe_{0.4}Bi_{2.6}$	~10	Yb_5Sb_3	1.1961(3)	0.9357(3)	0.8064(3)	5.2
4	'$Tb_6Fe_{0.5}Mn_{0.5}Bi_2$'	$Tb_6Fe_{0.5}Mn_{0.5}Bi_2$	~91	Fe_2P	0.82838(6)		0.42473(2)	5.6
		$Tb_5Fe_{0.22}Mn_{0.08}Bi_{2.7}$	~9	Yb_5Sb_3	1.2020(4)	0.9349(3)	0.8109(3)	6.2

[a-] the estimated standard deviations the phase composition (ESD) of 0.5 at.% for gadolinium and terbium, 1 at.% for Mn, Fe and Bi.